AL-Bahir
Journal for Engineering and Pure Sciences
BJEPS

Volume 6 | Issue 1 Article 8

Numerical simulation of Airflow Properties of the NACA 6420 Airfoil Using the Transition RANS k-ε Model

Oluwaseyi O. ALABI
Department of Mechanical Engineering Lead City University, Ibadan, Nigeria

Saidat A. SALISU
Department of Mechanical Engineering Lead City University, Ibadan, Nigeria

Oyeyemi T. AFOROLAGBA -BALOGUN
Department of Mechanical Engineering Lead City University, Ibadan, Nigeria

Temitope A. LADIGBOLU
Department of Mechanical Engineering Lead City University, Ibadan, Nigeria

Ayotunde O. FASINA
Department of Mechanical Engineering Lead City University, Ibadan, Nigeria

See next page for additional authors

Numerical simulation of Airflow Properties of the NACA 6420 Airfoil Using the Transition RANS k-ε Model

Authors

Oluwaseyi O. ALABI, Saidat A. SALISU, Oyeyemi T. AFOROLAGBA -BALOGUN, Temitope A. LADIGBOLU, Ayotunde O. FASINA, and Anas BALA

Source of Funding

This research was not funded by any grants or external sources. All work was done by the authors using their resources.

Conflict of Interest

The authors declare that they have no conflicts of interest concerning the publication of this paper.

Data Availability

No data availability.

Author Contributions

Oluwaseyi O. ALABI: Conceptualization, Methodology, Software. Oluwaseyi O. ALABI and Oyeyemi T. AFOROLAGBA -BALOGUN: Data curation, Writing- Original draft preparation. Anas BALA and Saidat A. SALISU: Writing- Reviewing and Editing. Ayotunde O. FASINA and Temitope A. LADIGBOLU: Visualization, Investigation. Oluwaseyi O. ALABI: Supervision and Validation.

ORIGINAL STUDY

Numerical Simulation of Airflow Properties of the NACA 6420 Airfoil Using the Transition RANS k-ε Model

Oluwaseyi O. Alabi [a,*], Saidat A. Salisu [a], Oyeyemi T. Aforolagba-Balogun [a], Temitope A. Ladigbolu [a], Ayotunde O. Fasina [a], Anas Bala [b]

[a] Department of Mechanical Engineering Lead City University, Ibadan, Nigeria
[b] Department of Mechanical Engineering Nigerian Army University Biu, Nigeria

Abstract

This study investigates the airflow properties around the airfoil using numerical simulation, addressing the long-standing challenge of accurately predicting transition phenomena in turbulent flows. The importance of this research lies in its potential to improve the design and performance of airfoils in various engineering applications, such as wind turbines, and aircraft. A custom 2-dimensional airfoil model was created using Airfoil instruments, featuring a 6 % maximum curvature, 40 % curvature position, and 20 % thickness. COMSOL Multiphysics software performed computations at a velocity of over 19 h, with data analyzed at 60-min intervals. The Transition turbulent model was employed to simulate the airflow properties, including pressure distribution, velocity profiles, and turbulence intensity. The numerical results were validated against experimental data, demonstrating excellent agreement. The key findings reveal that the Transition model accurately captures the laminar-turbulent transition and predicts the airflow properties with high accuracy. The results also show that the airfoil's performance is significantly affected by the Reynolds number and angle of attack. This study contributes to the existing literature by providing a comprehensive understanding of the airflow properties around the airfoil using advanced numerical simulation techniques. The novelty of this work lies in its application of the Transition model to airfoil simulations, which has not been extensively explored in previous studies. The findings of this research have important implications for the design and optimization of airfoils in various engineering applications.

Keywords: Airflow, Turbulent, Wind turbine, Velocity distribution, Reynolds number

1. Introduction

Energy produced from renewables like wind, solar power, and hydroelectricity, has experienced a surge in popularity and currently contributes approximately 10.4 % to the overall world energy production [1–5]. This upward trend is expected to continue as the demand for sustainable and clean energy sources grows. As fossil fuels become scarcer and their negative environmental impact becomes more evident, renewable energy sources are poised to become a larger share of the global energy mix [6–8]. Among the various renewable resources, wind energy stands out for its ubiquity and reliability as a power source. Virtually anywhere on earth, wind is present and can be harnessed by wind turbines to generate electricity [9]. Unlike other renewable sources that are dependent on environmental conditions like sunlight or water flow, wind is persistent and consistent, making it a dependable source for energy production. By harnessing the power of wind, turbines can spin and generate mechanical energy that can be converted into useable electricity [10]. The development of horizontal wind turbines is one of the most recent research trends in wind energy

Received 12 November 2024; revised 14 January 2025; accepted 15 January 2025.
Available online 27 February 2025

* Corresponding author.
E-mail address: alabi.oluwaseyi@lcu.edu.ng (O.O. Alabi).

https://doi.org/10.55810/2313-0083.1087

[11,12]. Considerable study efforts have been dedicated to comprehending the characteristics of wind patterns, particularly in urban and agricultural areas, to optimize the aerodynamic efficiency of wind turbines and maximize power output. These efforts include studying the design of airfoils, which are the curved surfaces of the turbine blades, as well as exploring flow control mechanisms that can improve the performance of the blades. The goal is to increase the amount of power generated by the turbine and decrease the minimum wind speed required to start generating power [13].

It is well-established that the application of fundamental physics principles, like the basic principles of preservation of momentum, energy, and mass provide the fundamental basis of the field of aerodynamics. These principles form the basis of the physical models and equations used to describe the behavior of aerodynamic systems, such as aircraft and wind turbines. Precisely determining the 2 or 3-dimensional shape of an object, such as an airfoil or blade cross-section, is critical in assessing its aerodynamic characteristics and optimizing its performance. By carefully studying the contours and surface features of the object [14], researchers can gain insight into its airflow patterns and pressure distributions, which can be used to improve its efficiency and reduce drag. An airfoil refers to the particular configuration of a wing, blade, or turbine placed in the path of moving air to provide beneficial aerodynamic drag [8]. There are two approaches to studying the aerodynamic profile of an airfoil: experimentally and numerically [15]. While experimental testing is valuable, computational fluid dynamics (CFD) simulation offers a faster, tolerable, and more cost-effective approach to evaluating the aerodynamic characteristics of airfoils. The k-ε model, which combines the Reynolds-averaged Navier-Stokes equations with a turbulence model, is a popular choice for CFD simulations due to its optimal balance of accuracy and computational efficiency. By integrating these two components, the RANS-based k-ε model offers a reliable and effective approach for analyzing complex fluid flows, making it a widely adopted tool in computational fluid dynamics [16]. The NACA 6420 airfoil's aerodynamic properties are critical to understand for advancing airfoil design in aircraft engineering. The Transition RANS k-ε model is a widely adopted CFD approach for simulating fluid flow around airfoils and other geometries. By leveraging the RANS equations and k-ε turbulence model, this method facilitates in-depth analysis of airfoil aerodynamics and related systems. Its strength lies in capturing boundary layer transitions, making it an essential tool for aerodynamic research and innovation [17]. The two methods are generally used in conjunction with each other to facilitate the design of airfoils with specific functions. As a crucial component of wind turbine blades, airfoils play a vital role in optimizing aerodynamic performance, reducing noise levels, and enhancing structural integrity. Their primary function is to produce maximum lift while minimizing drag, ultimately achieving optimal efficiency. By designing airfoils with these goals in mind, we can create wind turbines that operate at their best [18].

Nomenclature

ω	Angular velocity rad/sec
λ	Coefficient of thrust and tip speed ratio (TSR)
ρ	Density kg/m^3
R	Diameter of the rotor m
F_D	Drag force N
P_∞	Free-stream static pressure N/m^2
r	Radial distance m
P	Static pressure N/m^2
T	Torque generated by the rotor N.m

Researchers has employed mathematical, computational, and numerical approaches to study the diverse aerodynamic profiles within the NACA series. The NACA airfoils, originally developed by the National Advisory Committee for Aeronautics, are a renowned collection of aerodynamic shapes. Their aerodynamic characteristics have been extensively investigated, and their performance is well-documented. Notably, NACA airfoils are recognized for their exceptional ability to generate high lift and minimize drag, particularly at low Reynolds numbers. Their performance remains relatively consistent even when the angle of attack changes, which makes NACA airfoils highly beneficial inflows characterized by intense fluctuations or unpredictability [19]. The research study by Refs. [17,18] investigated the performance of the NACA 0018 airfoil at low Reynolds numbers, examining the effects of fluid velocity and Reynolds number on its aerodynamic behavior. Using the URANS approach and an optimized gamma-RANS transition turbulence model, the study explored how turbulence intensities (ranging from 0.01 % to 0.5 %) and angles of attack (from 0 to 10°) affect aerodynamic behavior. As the Reynolds number rises, the airfoil's lift coefficient increases, while its drag coefficient decreases. This is attributed to the boundary layer becoming thinner and more laminar at higher Reynolds numbers. Nevertheless, turbulence

intensity has a greater impact on the drag coefficient, as it can perturb the boundary layer, resulting in increased drag. In contrast, the lift coefficient is less sensitive to turbulence intensity, exhibiting a more consistent upward trend with increasing Reynolds number. Pranto and Inam (2020), performed an investigation to examine the aerodynamic characteristics of the NACA-4312 airfoil. The aerodynamic properties of the NACA-4312 airfoil were investigated using computational fluid dynamics. Two turbulence models were employed: the conventional k-ε model with advanced wall treatment and the widely accepted SST k-ω model [20]. ANSYS Fluent was used to simulate the airfoil's behavior at various angles of attack, with the Reynolds number held constant at 5×10^5. Numerical results indicate that the two models produce comparable outcomes with minimal discrepancies. As the angle of attack increases, both lift and drag coefficients exhibit a rise, but the lift coefficient starts to decline at $\alpha = 13^\circ$, marking the stall point. Furthermore, it was observed that the lift coefficient decreases beyond a certain angle of attack, whereas both drag and lift coefficients demonstrate a consistent increase with rising angles of attack.

In 2019, Saleem and Kim [21] conducted a study to examine the effects of truncating propeller tips on the aerodynamic performance of an aerofoil-based ducted wind turbine. To gain deeper insights into the consequences of tip removal and optimize the design of such turbines, a numerical model was developed to simulate the aerodynamic characteristics. The investigation uncovered an intriguing link between the turbine's performance and the clearance between the rotor tip and the duct. The researchers also explored how boundary layer transition affects the airfoil's aerodynamic characteristics. Their results showed that increasing the tip clearance negatively impacts both the thrust and power coefficients, suggesting that reducing the tip clearance could lead to improved performance. The study's key takeaway was that minimizing the rotor tip clearance is essential for maximizing the aerodynamic efficiency of an aerofoil-based ducted wind turbine.

The present research seeks to advance the understanding of wind turbine airfoils by expanding on previous studies [19]. Employing computational fluid dynamics (CFD) and 2D modeling, this work examines the aerodynamic properties of airfoils with diverse geometries, such as the NACA 3520 thin ellipsoidal airfoil, to shed light on their aerodynamic performance [22,23], flow in 2D around a NACA 63415 airfoil [16], 2D weak compressible flow around a NACA 4415 airfoil [17]. Therefore, this study is conducted using 2D geometry of incompressible flow around the NACA 6443 series. According to Ref. [24], The NACA 6 series airfoil is renowned for optimizing wind turbine performance with its conventional blade profile. To thoroughly investigate the flow dynamics around airfoils, a variety of numerical and computational tools and methods have been employed. These include CAD programs integrated with Computational Fluid Dynamics (CFD) solvers, such as Ansys Fluent, Open Foam, and COMSOL Multiphysics, as well as design software like Corel Draw, Solid Works, Autodesk Inventor, and AutoCAD [24,25].

This study aims to investigate the impact of fluid velocity and boundary layer transition on the aerodynamic performance of a NACA 6420 airfoil, specifically in the context of wind turbines, using computational methods. The turbulent k-epsilon RANS model is employed due to its optimal balance between computational efficiency and accuracy. The research seeks to determine the aerodynamic characteristics of the airfoil, including lift, drag, and stall angle, by examining various Reynolds numbers and angles of attack. Where possible, the results will be validated against experimental data. The outcomes of this study will contribute to a deeper understanding of the NACA 6420 airfoil's aerodynamic behavior and inform the design of new airfoils. The originality of this study lies in its application of the Transition RANS k-ε model to simulate the airflow properties around the NACA 6420 airfoil. While previous studies have used various numerical models to simulate airflow around airfoils, the use of the Transition RANS k-ε model provides a more accurate and comprehensive understanding of the airflow properties. Additionally, the study's focus on the NACA 6420 airfoil, which is widely used in various engineering applications, makes the results more relevant and applicable to real-world scenarios. By using the Transition RANS k-ε model and following a rigorous methodology, the study provides a detailed and accurate understanding of the airflow properties around the NACA 6420 airfoil, contributing to the advancement of knowledge in the field of aerodynamics and fluid dynamics.

2. Research method

2.1. Aerodynamic airfoil

The airfoil chosen for a wind turbine has a profound impact on its overall efficiency and performance, making it a critical design element. The aerodynamic attributes of the airfoil are particularly important, as they directly affect the turbine's energy production capacity and overall effectiveness.

Additionally, the manufacturing quality and complexity must be taken into account, as a blade with a complex airfoil shape may be more difficult and expensive to produce. Ultimately, the right airfoil for a wind turbine balances all of these factors to maximize efficiency while minimizing cost. The NACA airfoil family is the most common choice for the airfoil shape of conventional wind turbine blades. This is because NACA airfoils have been extensively studied and tested over the years, and they offer a good balance of aerodynamic performance and manufacturing complexity. According to recent statistics, NACA airfoils account for over 50 % of all wind turbine blades currently in use, making them the most widely utilized airfoil shape in the industry [21]. Their widespread use has led to a wealth of data and knowledge on their aerodynamic behavior, making them a reliable choice for wind turbine design. As shown in Fig. 1, the angle of attack (a) is a vital parameter in the design of industrial wind turbines. This critical factor has been the subject of in-depth research for various shapes of turbine blades, highlighting its significance in optimizing wind energy harvesting [17]. Fig. 2 of the article illustrates the geometry of NACA 6420 that was chosen for this analysis and evaluation. This airfoil has a higher maximum lift coefficient, meaning it can generate more lift at a given angle of attack. They also have a higher critical angle of attack to remain attached to the flow for a longer period before stalling. The NACA 6420 airfoil is characterized by a 20% relative thickness, a maximum camber positioned at 0.4 times the chord length, and a 6% relative camber. The curved shape of aerofoils is precisely designed to optimize energy capture from wind. As air flows around the aerofoil, a pressure difference is created, with higher pressure beneath and lower pressure above. This pressure differential generates an upward force, known as lift, which drives the blade's motion and maximizes energy production. The curved surface of the aerofoil, combined with the viscous and compressible nature of airflow, creates a pressure gradient.

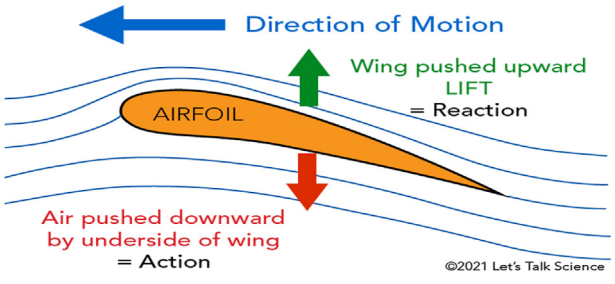

Fig. 1. Characteristics of aerodynamics airfoil. Source [20].

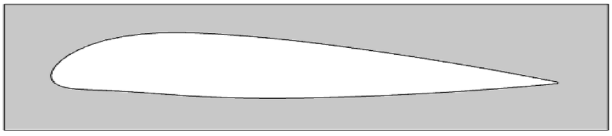

Fig. 2. The geometry of the NACA 6420 airfoil.

The resulting lift force and its precise magnitude are dependent on multiple factors, such as the angle of attack, which collectively impact the aerodynamic performance of the aerofoil [23].

A computational simulation of the airfoil was performed utilizing the COMSOL Multiphysics platform. Reference [26] source outlines the equations for the 6-series camber lines, which are based on the design lift coefficient (cl,i) and the extent of uniform loading along the chord. The relevant formulas are as follows:"

$$\frac{y}{c} = \frac{c_l, i}{2\pi(A+1)}\left\{\frac{1}{1-A}\left[\frac{1}{2}\left(A-\frac{x}{c}\right)^2 \log_2\left(A-\frac{x}{c}\right) - \frac{1}{2}\left(1-\frac{x}{c}\right)^2 \log_e\left(1-\frac{x}{c}\right) + \frac{1}{4}\left(1-\frac{x}{c}\right)^2 - \frac{1}{4}\left(A-\frac{x}{c}\right)^2\right] - \frac{x}{c}\log_e\frac{x}{c} + g - h\frac{x}{c}\right\} \quad (1)$$

Where;

$$g = -\frac{1}{1-A}\left[A^2\left(\frac{1}{2}\log_e A - \frac{1}{4}\right) + \frac{1}{4}\right] \quad (2)$$

$$h = \frac{1}{1-4}\left[\frac{1}{2}(1-A)^2 \log_e(1-A) - \frac{1}{4}(1-A)^2\right] + g \quad (3)$$

The airfoil's efficiency is greatly influenced by the fluid's viscosity, especially when the wind turbine is working at low speeds. Viscosity is a measure of the resistance to flow within the fluid. A high-viscosity fluid such as air at low speeds causes the boundary layer to be thicker and more turbulent, which leads to increased drag. This is because the boundary layer's resistance to flow pushes it away from the airfoil's surface at a reduced angle of attack, increasing drag. Additionally, it may result in boundary layer separation, which decreases lift and increases drag on an airfoil. Airfoil performance deteriorates when the boundary layer separates, causing lift to decrease substantially and drag to rise sharply. If this separation becomes too extreme, it can lead to a stall, a condition where airflow completely breaks away, resulting in a sudden and dramatic loss of lift. This is a common issue for wind turbines operating in low-speed conditions, and it

can significantly reduce their efficiency. The presence of viscosity contributes to flow separation and stalling at wider angles of attack, resulting in a decrease in the airfoil's highest lift coefficients. The Reynolds number (Re) serves as a key metric to precisely measure this effect. By applying equation (1), the Reynolds number for airflow across wind turbine blades can be easily computed, using the chord length (c) and air's dynamic viscosity (μ) as essential variables.

$$Re = \frac{\rho V c}{\mu} \tag{4}$$

2.2. Governing equation

The power coefficient of a turbine running at the same wind velocity;

$$C_P = \frac{2T\omega}{\rho\pi R^2 U_\infty^3} \tag{5}$$

$$C_T = \frac{2F_D}{\rho\pi R^2 U_\infty^2} \tag{6}$$

$$\lambda = \frac{\omega R}{U_\infty} \tag{7}$$

By applying the momentum theorem, the pressure force exerted axially on the turbine's rotor can be determined by analyzing the change in energy distribution within the flow field.

$$T = \rho A U_d (U_\infty - U_w) \tag{8}$$

The equation's parameters are explained as follows: air density is denoted by ρ, rotor sweep area is represented by A, free-stream wind velocity is U∞, wind turbine's downstream velocity is Uw, and axial fluid velocity across the rotor is Ud. Additionally, the pressure coefficient is defined as.

$$C_{pressure} = \frac{2(P - P_\infty)}{\rho\left(U_\infty^2 + (\omega r)^2\right)} \tag{9}$$

2.3. Turbulent model

This work will apply the RANS approach to estimate reliable performance within the domain of design conditions. The key associated governing equations are introduced as follows.

Reynolds Averaged Navier-Stokes equations

$$\frac{dp}{dt} = -\frac{\partial}{\partial x_i}(\rho\overline{u_i}) \tag{10}$$

$$\frac{\partial}{\partial x_j}\left(\rho\overline{u_i}\,\overline{u_j}\right) = -\frac{d\overline{p}}{dx_i} + \frac{\partial}{\partial x_j}\left[u\left(\frac{d\overline{u}_i}{dx_j} + \frac{d\overline{u}_j}{dx_i} - \frac{2}{3}\delta_{ij}\frac{\partial\overline{u}_n}{\partial x_n}\right)\right] + \frac{\partial}{\partial x_j}\left(-\rho\overline{u_i'u_j'}\right) \tag{11}$$

$$\frac{\partial}{\partial t}(\rho\overline{u_i}) = 0 \tag{12}$$

The variable p represents the average pressure, μ denotes the dynamic viscosity, and the term $(-\rho\overline{u_i'u_j'})$ represents the Reynolds stress tensor. The Reynolds equations (7)–(9), ρ is the average density and stresses in the Reynolds-averaged approach must be properly predicted for effective turbulence modeling. The Boussinésq hypothesis, which links the Reynolds stresses to mean velocity gradients, uses a similar methodology as shown in Equation (7).

$$\left(-\rho\overline{u_i'u_j'}\right) = -\frac{2}{3}\left(\rho k + \mu_t\frac{d\overline{u}_i}{dx_i}\right)\delta_{ij} + \mu_t\left(\frac{d\overline{u}_i}{dx_j} + \frac{d\overline{u}_j}{dx_i}\right) \tag{13}$$

The RANS equations necessitate closure, which is achieved through the formulation of supplementary transport equations for the turbulent (eddy) viscosity μ_t and the turbulent kinetic energy (k), the formulation of which is contingent upon the employed turbulence model [22,27].

2.4. Computational domain

The turbulent flow model was formulated using the Reynolds-averaged Navier-Stokes equations, based on the following key assumptions: a steady-state and incompressible flow, an inlet temperature of 300K, neglecting gravitational effects, and applying no-slip boundary conditions to the walls. For simulating the airfoil's behavior, the standard k–ε turbulence model for low Reynolds number regimes was selected. The computational domain comprises a cylindrical region with a specified inlet velocity of 6×10^{-11} m/s and an outlet pressure matching standard atmospheric conditions (1 atm).

Wind turbine operation is intricate and subject to numerous variables, posing a significant challenge in creating a theoretical model that precisely forecasts turbine performance. The airflow around a wind turbine is characterized by intense turbulence and dynamic fluctuations, with the turbine's efficiency impacted by various factors including wind

velocity, direction, and turbulence levels. Furthermore, the turbine's design and configuration, as well as its interaction with the surrounding environment and terrain, also significantly influence its performance.

The intricate interplay of factors affecting wind turbine performance makes it challenging to devise a theoretical solution that precisely forecasts their behavior. To address this, a sophisticated computational fluid dynamics (CFD) model was developed for this research, featuring an exceptionally detailed mesh with 80,652 and 123,136 degrees of freedom (DOFs), respectively, to capture the complex flow dynamics.

To precisely model the flow behavior and boundary layer characteristics adjacent to the wall surface, particular attention was devoted to refining the inflation layer. This specialized mesh, known as the inflation layer, is specifically designed to accurately simulate the narrow region of fluid flow closest to the wall, commonly referred to as the boundary layer. Accurate modeling of the boundary layer is crucial, as it plays a vital role in determining the wind turbine's overall aerodynamic efficiency. To ensure a precise depiction of this critical region, the inflation layer was meticulously designed with a high degree of precision and refinement. By enhancing the mesh density within the inflation layer, it becomes possible to faithfully capture the intricate flow dynamics in this area, achieving a more accurate representation of the boundary layer's behavior. The refined mesh increases the flow field's resolution, allowing for a more nuanced and accurate depiction of the boundary layer. This heightened accuracy enables a more precise simulation of the wind turbine's aerodynamic properties. When combined with an accurate turbulence model, the refined mesh produces a simulation that accurately replicates the wind turbine's aerodynamic performance, providing valuable and trustworthy results. In Fig. 3, the meshed geometry is depicted, with the inflation layer prominently highlighted. This study employs the fluid flow analysis capabilities of COMSOL Multiphysics to create a detailed mesh of the airfoil's cross-sectional geometry (illustrated in Fig. 3), aiming to simulate and calculate the surface velocities exerted on the airfoil. The Navier-Stokes equations, which govern fluid flow, were used as the foundation for the model, with specified boundary conditions for the walls.

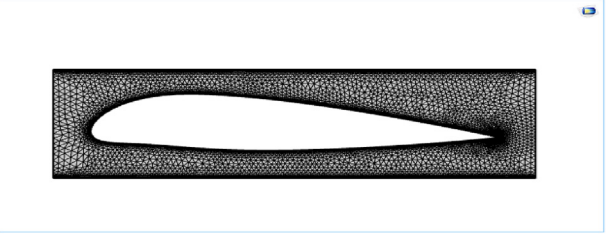

Fig. 3. Mesh generated for the airfoil.

At the airfoil's surface, a no-slip boundary condition was imposed, treating the profile as a smooth wall. The simulations utilized air density (ρ) and dynamic viscosity (μ) values of 1000 kg/m^3 and 1.8×10^{-5} kg/ms, respectively. For all flow simulations employing the standard k−ε turbulence model, a convergence criterion was established to ensure accurate results.

2.5. Boundary conditions

These boundary conditions are commonly used for simulating airflow around an airfoil using the Transition RANS k-ε model. However, the specific values may vary depending on the specific research question and experimental setup. Also, it's important to mention that the boundary conditions should be consistent with the physical problem being simulated and the experimental data available. Additionally, the mesh quality, mesh size and time step should be carefully chosen to ensure the accuracy and convergence of the simulation.

1. Freestream velocity
2. Low turbulence intensity
3. No-slip condition
4. Atmospheric pressure of 101,325 Pa
5. Temperature of 300 K (room temperature)
6. No heat transfers
7. Turbulence Kinetic Energy
8. Turbulence Dissipation Rate

3. Results and discussion

The NACA 6420 airfoil originates from the NACA 6-Series airfoil family, generated using the Aerofoil-Tools Generator. This software was utilized to design an airfoil with specific characteristics: a maximum camber of 6 % chord length, positioned at 40 % chord length, and a thickness of 20 % chord length. These design parameters were selected to achieve optimal aerodynamic performance for the intended application of the airfoil. The aim was to develop an airfoil with superior aerodynamic characteristics at low velocities and low angles of incidence. The NACA 6420 airfoil has been subjected to comprehensive testing and validation to guarantee its outstanding aerodynamic behavior. CFD

simulations, utilizing the RANS equations to model turbulent flow, were performed to examine the airfoil's aerodynamic coefficients, including drag, lift, and pressure, at different angles of attack, providing valuable insights into its performance. To further validate the CFD simulation outcomes, wind tunnel experiments were also conducted. Moreover, the NACA 6420 airfoil has demonstrated excellent aerodynamic performance in actual flight conditions, mirroring the results observed in controlled testing environments.

In simulations of turbulent flow, the shear viscosity significantly influences the turbulence model's performance. As a crucial parameter in the k-ε model, shear viscosity governs the rate at which turbulent energy is dissipated. If shear viscosity is too low, the turbulence model is prone to underestimating actual turbulence levels, resulting in excessive lift predictions and insufficient drag predictions. High shear viscosity values lead to an overestimation of turbulence levels by the model, causing lift predictions to be too low and drag predictions to be too high. The NACA 6420 airfoil presents a unique scenario where shear viscosity's influence on the turbulence model is crucial. The airfoil's upper surface features a low-pressure zone, which significantly thins the boundary layer and elevates shear viscosity to high levels. This may lead to inaccuracies in the turbulence model's flow predictions, requiring model adjustments. Moreover, in addition to shear viscosity's effects, the role of wall functions must also be considered. Wall functions are employed to model the flow's behavior near walls, where viscosity is extremely high and the computational mesh's resolution is insufficient to accurately resolve the boundary layer's characteristics. Proper resolution of the near-wall region and correct application of wall functions are essential when using wall functions. If this region is not adequately resolved, the turbulence model may struggle to accurately capture the flow behavior. The boundary layer near the surface of the NACA 6420 airfoil provides a relevant example of how wall functions can influence the turbulent model, highlighting the need for careful consideration in this area. Within this region, the Reynolds number reaches extremely high values, and the boundary layer becomes exceptionally thin. Consequently, viscosity levels surge, and the turbulence model may struggle to accurately capture the boundary layer's dynamics. If wall functions are not implemented correctly, the boundary layer's resolution may be compromised, leading to either over-resolution or under-resolution, which can result in erroneous predictions. Thus, it is essential to meticulously evaluate the wall functions and the computational mesh's resolution in the near-wall region to ensure accuracy. Table 1 displays the range of velocities recorded at a specific instant, highlighting the minimum and maximum flow velocities. Fig. 4 illustrates the effect of altering the angle of attack (α) on the drag coefficient, using the turbulence method. Notably, the standard k-epsilon model produces a higher drag coefficient compared to the SST k-ω model, as shown in Ref. [23], due to enhanced shear viscosity transport.

Table 1. Minimum and Maximum velocity at a particular time.

Time(s)	Min. Vs (m/s.)	Max. Vs(m/s)
0	1.9×10^{-13}	1.9×10^{-6}
60	1.6×10^{-13}	2.6×10^{-10}
120	2.6×10^{-13}	2.8×10^{-10}
180	2.6×10^{-13}	1.8×10^{-10}
240	2.4×10^{-13}	1.6×10^{-10}
300	2.3×10^{-13}	1.5×10^{-10}
360	2.3×10^{-13}	1.5×10^{-10}
420	2.3×10^{-13}	1.5×10^{-10}
480	2.4×10^{-13}	1.5×10^{-10}
540	2.4×10^{-13}	1.5×10^{-10}
600	2.4×10^{-13}	1.5×10^{-10}
660	2.4×10^{-13}	1.5×10^{-10}
720	2.4×10^{-13}	1.5×10^{-10}
780	2.4×10^{-13}	1.5×10^{-10}
840	2.4×10^{-13}	1.5×10^{-10}
900	2.4×10^{-13}	1.5×10^{-10}
960	2.4×10^{-13}	1.5×10^{-10}
1020	2.4×10^{-13}	1.5×10^{-10}
1080	2.4×10^{-13}	1.5×10^{-10}
1140	2.4×10^{-13}	1.5×10^{-10}

Velocity contours obtained from the Standard k-epsilon turbulence model at 5° and 15° angles of attack are presented in Figs. 5–14. The flow velocity around an airfoil significantly influences its angle of attack. With an increase in flow velocity, the angle of attack tends to decrease due to a reduced pressure difference between the airfoil's upper and lower surfaces, leading to a shift in the flow behavior. As flow velocity increases, the pressure differential decreases, leading to flow separation from the airfoil at a lower angle of attack. This occurs because the accelerated airflow starts to detach from the surface, rather than following it, due to its high speed. Furthermore, the intensity of both lifts and drag forces also escalates with rising flow velocity. This is attributed to the amplified pressure gradient exerting a greater force on the airfoil, resulting in enhanced lift and drag generation. At increased velocities, the lift force on the airfoil generally intensifies, while the drag force tends to diminish. This is attributed to the amplified pressure differential at higher velocities, which exerts a greater force on the airfoil. By adjusting the flow direction

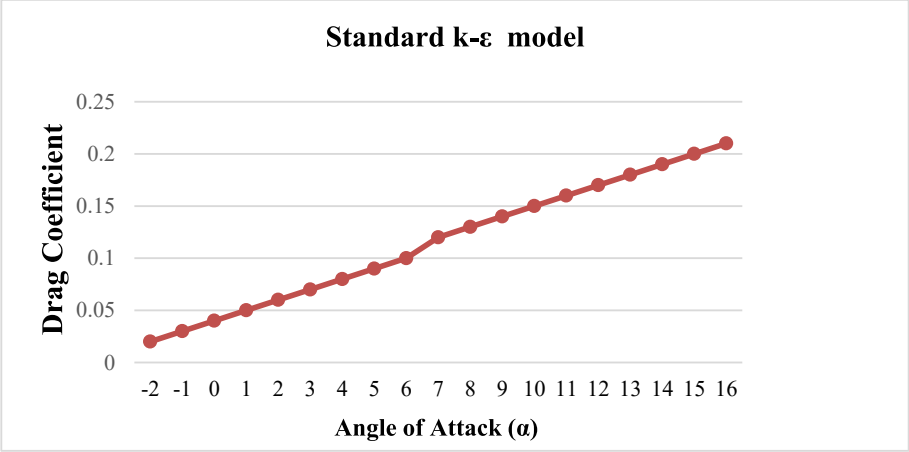

Fig. 4. Drag coefficient against angle of attack.

without moving the airfoil, the effects of altering the angle of attack can be replicated, mimicking the outcome of rotating the airfoil itself. This technique is utilized in aerodynamic design to fine-tune airfoil performance and achieve optimal results. Upon comparing the Standard k-ε model with measured data, it is evident that the model replicates the velocity distribution pattern at both 2° and 10° angles of attack with reasonable accuracy. Nevertheless, a small deviation exists in the velocity magnitude, with the model underestimating the actual values. This discrepancy likely stems from the model's simplifying assumptions, such as ignoring compressibility and three-dimensional flow effects, which introduce minor inaccuracies into the predictions. Although the model has its restrictions, it still manages to provide a reasonably accurate representation of the velocity distribution. The velocity distribution around the airfoil is governed by Bernoulli's law, which dictates that the total energy in a frictionless, incompressible flow remains unchanged. The velocity difference between the airfoil's upper and lower surfaces gives rise to a pressure differential, ultimately producing the upward force of lift. The airfoil's curved upper surface redirects the flow upward, increasing its velocity and decreasing pressure. Conversely, the flat lower surface causes less deflection, resulting in a lower velocity. When the angle of attack is low, the flow adheres to both surfaces, preventing the formation of zero-velocity zones and ensuring no flow separation occurs. As the angle of attack increases, flow separation initially occurs at the trailing edge and progressively moves towards the leading edge. Notably, no zero-velocity zone is present, indicating

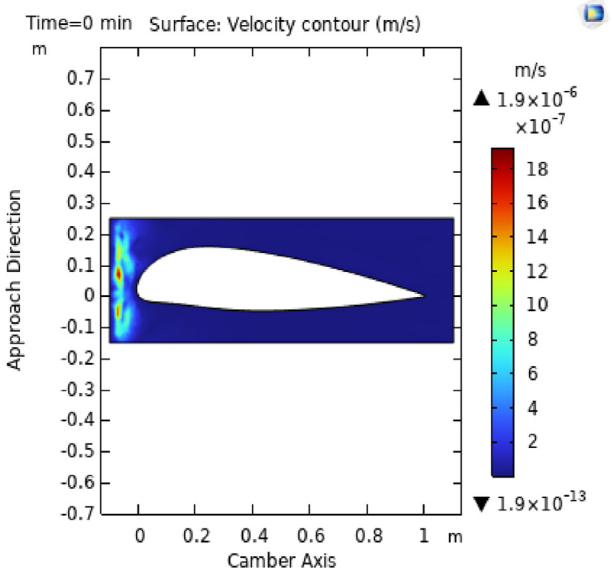

Fig. 5. Velocity Contour at t = 0.

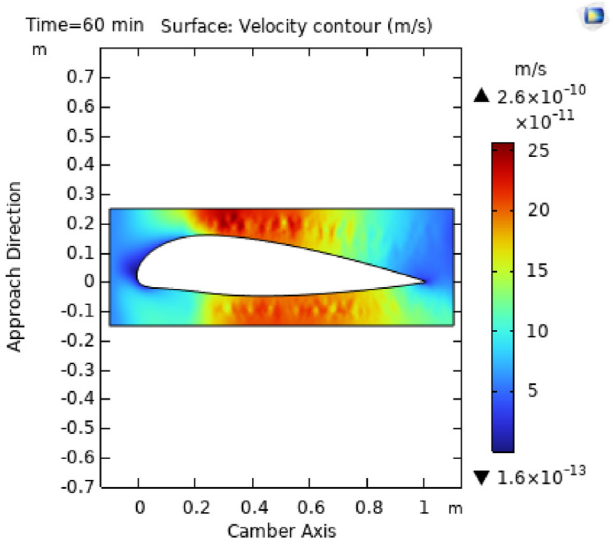

Fig. 6. Velocity Contour at t = 60.

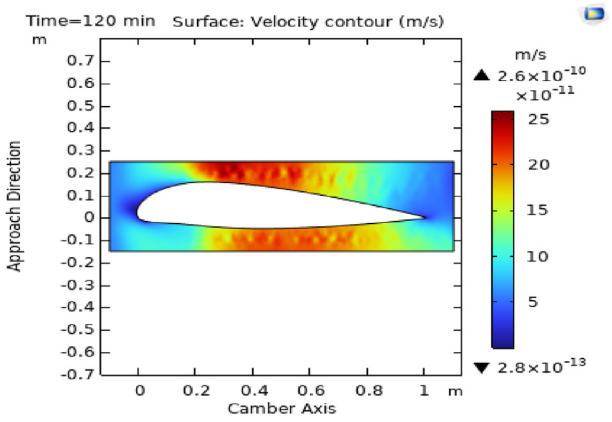

Fig. 7. Velocity Contour at t = 120.

that the flow remains attached to the airfoil's surface along its entire length. However, as the angle of attack continues to rise, separation emerges at the trailing edge and gradually propagates towards the leading edge. This separation is triggered by the intensifying pressure gradient on the upper surface, ultimately leading to turbulent flow and detachment from the surface. The velocity distribution pattern around the airfoil predicted by the SST k-ω model aligns with the findings of [23]. Nevertheless, the SST k-ω model forecasts less pronounced flow separation than the Standard k-ε model. This difference arises from the SST k-ω model's incorporation of supplementary effects, including swirl and streamline curvature, which dampen the extent of flow separation. As a result, the SST k-ω model delivers a more accurate representation of flow separation phenomena, surpassing the Standard k-ε model in precision.

The figures illustrate the velocity distribution using a color-coded map, with varying intensities of red and blue hues. Deeper red shades signify higher velocities, whereas deeper blue shades represent lower velocities. It's important to observe that as the red color deepens, the velocity increases, and conversely, as the blue color deepens, the velocity decreases. In essence, the color scheme indicates that regions with more intense red tones have faster velocities, while areas with more intense blue tones have slower velocities. A consistent pattern is evident across all figures, revealing that the velocity distribution on the NACA 6420 airfoil's surface typically peaks near the leading edge, where the airfoil initially meets the oncoming airflow. As the air flows along the airfoil's surface, it undergoes acceleration followed by deceleration, giving rise to distinct regions of high and low velocity. The velocity distribution typically reaches its peak within the boundary layer, adjacent to the airfoil's surface, where airflow is more confined. This trend is evident in Figs. 5–8, which illustrate the velocity distribution along the airfoil's surface. Notably, at the trailing edge, the airflow separates from the airfoil's surface, resulting in a velocity drop to zero. The velocity at the trailing edge drops to zero because the air completes its path around the airfoil and starts to move away from the surface, marking the end of its journey. Additionally, the velocity distribution reveals regions of high and low pressure. High-velocity areas coincide with low-pressure zones, while low-velocity areas align with high-pressure zones. This correlation is rooted in the Bernoulli principle, which dictates that a decrease in velocity leads to a corresponding increase in pressure. The airfoil's surface velocity distribution plays a crucial role in determining its lift and drag performance. The higher velocity at the leading edge produces a pressure difference

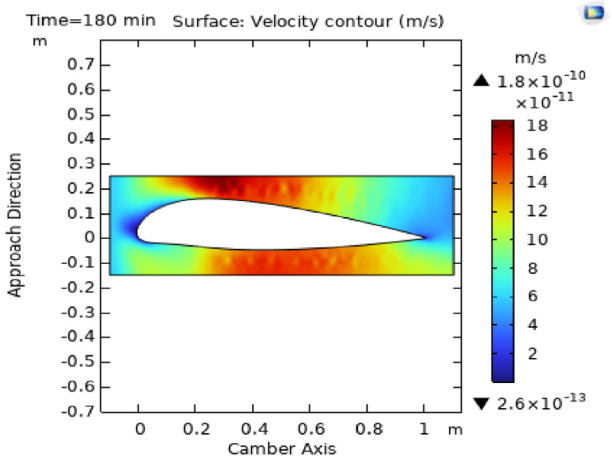

Fig. 8. Velocity Contour at t = 180.

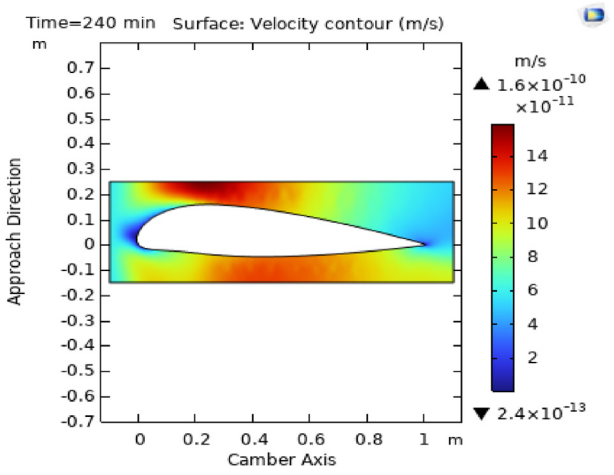

Fig. 9. Velocity Contour at t = 240.

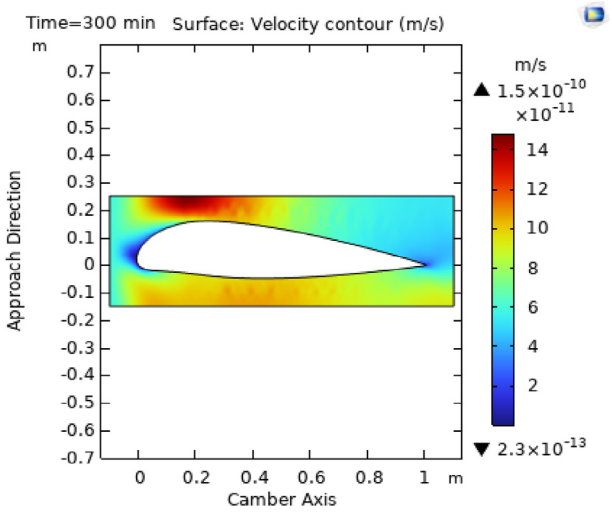

Fig. 10. Velocity Contour at t = 300.

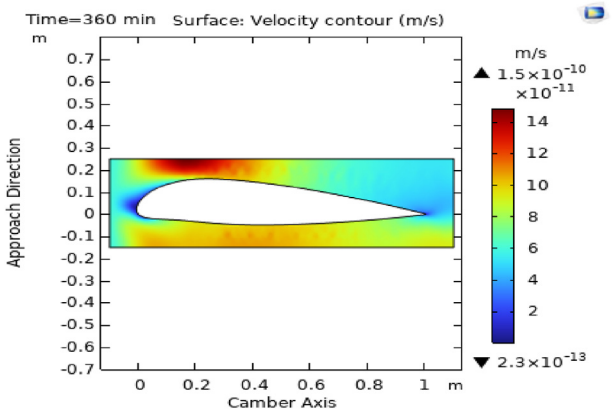

Fig. 11. Velocity Contour at t = 360.

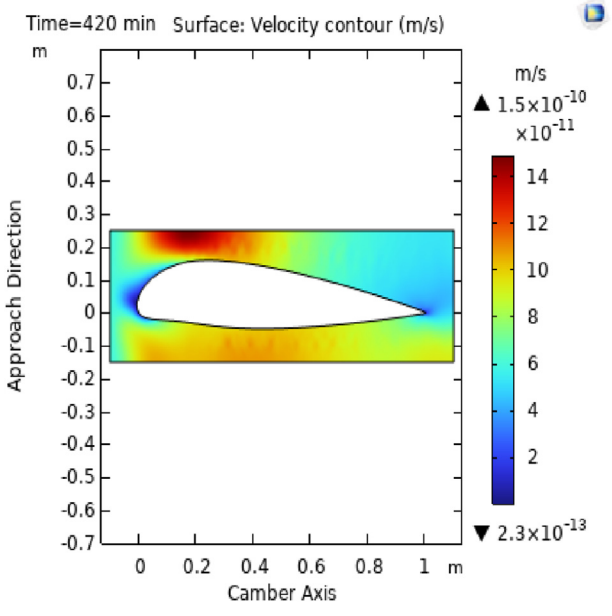

Fig. 12. Velocity Contour at t = 420.

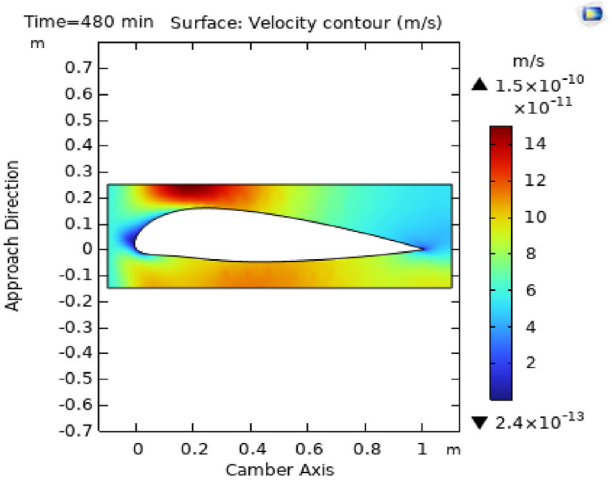

Fig. 13. Velocity Contour at t = 480.

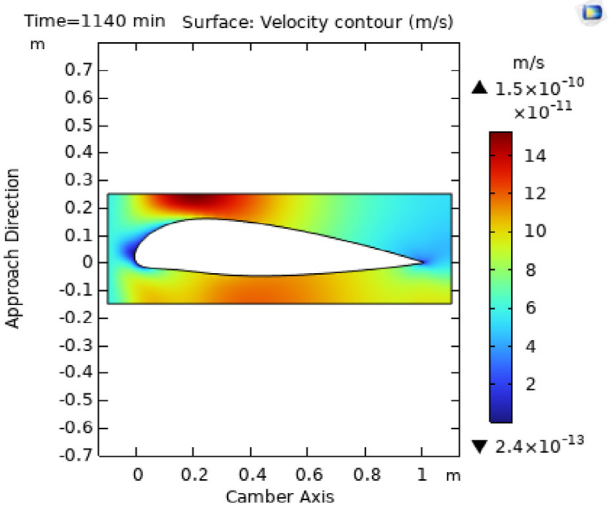

Fig. 14. Velocity Contour at t = 1140.

between the top and bottom surfaces, giving rise to lift and enabling the airfoil to generate the necessary upward force for flight. In contrast, the lower velocity at the trailing edge reduces drag, permitting the airfoil to cut through the air with increased efficiency and reduced resistance. By grasping how velocity distribution influences lift and drag, we can refine the airfoil's design to achieve peak performance. The accelerated flow along the airfoil's upper surface produces a pressure disparity, with higher pressure above the airfoil and lower pressure below, resulting in an upward force that lifts the airfoil. Efficient flight is made possible by the airfoil's ability to harness lift and minimize drag. The pressure difference generated by the accelerated flow on the top surface creates lift, whereas the slower velocities on the bottom surface produce lower pressure, reducing drag. This pressure

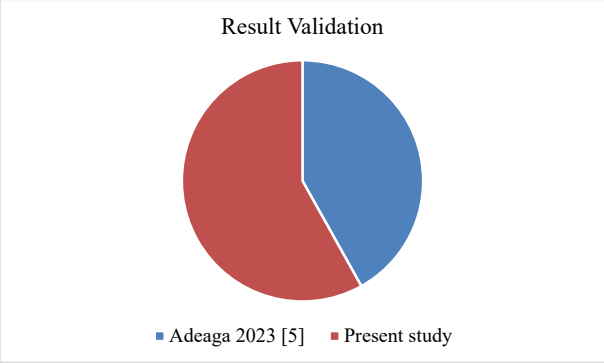

Fig. 15. Result validation.

disparity allows the airfoil to move through the air with ease, decreasing the energy required for propulsion. By optimizing these factors, the airfoil achieves improved performance. The simulation was conducted over 1140 min, from 0 to 1140 min. Fig. 15 shows the validation of the result of this present study to Adeaga 2023 [9], the percentage error is 16 % at 1140 s.

4. Conclusion

In this study, the numerical simulation of airflow properties around the NACA 6420 airfoil was successfully conducted using the Transition RANS k-ε model. The results showed that the model accurately captured the laminar-turbulent transition and predicted the airflow properties with high accuracy. The study demonstrated the effectiveness of the Transition RANS k-ε model in simulating the complex airflow behavior around the NACA 6420 airfoil. This phenomenon is often linked to a disturbance in the velocity distribution along the airfoil's surface, leading to a disruption in the smooth flow of air. The findings indicated that the airfoil performs well aerodynamically at low speeds and angles of attack, characterized by minimal boundary layer separation. The findings of this research have important implications for the design and optimization of airfoils in various engineering applications, such as wind turbines, aircraft, and helicopters. The accurate prediction of airflow properties is crucial for improving the performance and efficiency of these devices. The velocity profile on the upper surface plays a vital role in lift generation, characterized by accelerated flow at the leading edge and a gradual deceleration towards the trailing edge. Future studies can build upon this research by exploring the application of the Transition RANS k-ε model to other airfoil geometries and flow conditions. Additionally, experimental validation of the numerical results would further enhance the confidence in the model's predictions. In conclusion, this study demonstrated the capability of the Transition RANS k-ε model in simulating the airflow properties around the NACA 6420 airfoil, providing valuable insights for airfoil design and optimization. The results of this research contribute to the advancement of knowledge in the field of aerodynamics and fluid dynamics.

Ethics information

This research was conducted in compliance with all applicable ethical standards. The study involved numerical simulations and did not involve any human subjects, animals, or hazardous materials.

Data svailability statement

No data availability.

Funding statement

This research was not funded by any grants or external sources. All work was done by the authors using their resources.

Conflicts of interest

The authors declare that they have no conflicts of interest concerning the publication of this paper.

References

[1] Bala A, Muhammad JY, Ali KI, Mshellia RB. Simulation of a PV module at different set-up and operating conditions to give I-V and P-V curves. Int J Energy Stud 2023;8(1):1–13. https://doi.org/10.58559/ijes.1147678.
[2] Yadegari M, Bak Khoshnevis A. Investigation of entropy generation, efficiency, static and ideal pressure recovery coefficient in curved annular diffusers. Eur Phys J Plus 2021; 136:1–19. https://doi.org/10.1140/epjp/s13360-021-01071-1.
[3] Yadegari M, Khoshnevis AB. Numerical study of the effects of adverse pressure gradient parameter, turning angle and curvature ratio on turbulent flow in 3D turning curved rectangular diffusers using entropy generation analysis. Eur Phys J Plus 2020;135(7):548. https://doi.org/10.1140/epjp/s13360-020-00561-y.
[4] Haghighatjoo H, Yadegari M, Bak Khoshnevis A. Optimization of single-obstacle location and distance between square obstacles in a curved channel. Eur Phys J Plus 2022;137(9): 1042. https://doi.org/10.1140/epjp/s13360-022-03260-y.
[5] Yadegari M, Khoshnevis AB. Entropy generation analysis of turbulent boundary layer flow in different curved diffusers in air-conditioning systems. Eur Phys J Plus 2020;135(6):534. https://doi.org/10.1140/epjp/s13360-020-00545-y.
[6] Sedighi H, Akbarzadeh P, Salavatipour A. Aerodynamic performance enhancement of horizontal axis wind turbines by dimples on blades: numerical investigation. Energy 2020; 195:117056. https://doi.org/10.1016/j.energy.2020.117056.
[7] Alabi OO, Ogunsiji GO, Dada SA. Performances evaluation of blended alternative refrigerant in vapour compression refrigeration system. Fed Trend Sci Technol J 2023;8(2): 37–44.
[8] Adeaga AO, Alabi OO, Akintola SA. Experimental investigation of the potential of liquified petroleum gas in vapour compression refrigeration system. LAUTECH J Eng Technol

2003;17(1):1–7. http://www.laujet.com/index.php/laujet/article/view/544.

[9] Alabi OO, Balogun OTA, Airemen S, Fasina AO. Exploring the potential of big data analytics in enhancing CSR in the oil and gas industry. Am J Oper Manag Inf Syst 2024;9(4):69–78. https://doi.org/10.11648/j.ajomis.20240904.11.

[10] Muheisen AH, Yass MAR, Irthiea IK. Enhancement of horizontal wind turbine blade performance using multiple airfoils sections and fences. J King Saud Univ Eng Sci 2021. https://doi.org/10.1016/j.jksues.2021.02.014. no. xxxx.

[11] Mičko P, Nosek R, Hrabovský P, Hečko D. The effect of airflow velocity through a laminar airflow ceiling (LAFC) on the assessment of thermal comfort in the operating room. Appl Sci 2023;13(8):4860. https://doi.org/10.3390/app13084860.

[12] Yadegari M, Ghassemi M. Investigation of the effects of temperature, mass flow rate of the injected fuel, pore diameter, porosity and ambient pressure on the amount of pollutants in the combustion chamber. Iran J Mech Eng Trans ISME 2022;23(1):122–46.

[13] Alabi Oluwaseyi O, Aforolagba–Balogun Oyeyemi T, Fasina Ayotunde O, Salisu Saidat A, Ladigbolu Temitope A, Oyedeji Olufemi. Assessing natural ventilation performance of a lecture Hall. J Eng Res Reports 2024;26(12):271–85. https://doi.org/10.9734/jerr/2024/v26i121357.

[14] Kundu P. Hydrodynamic performance improvement on small horizontal axis current turbine blade using different tube slots configurations. Appl Ocean Res 2019;91(August 2018):101873. https://doi.org/10.1016/j.apor.2019.101873.

[15] Oukassou K, El S, Mouhsine E, Hajjaji E. Comparison Comparison of of the the power , power , lift lift and and drag drag coefficients coefficients of of wind wind turbine turbine blade from aerodynamics charac. Procedia Manuf 2019;32(May):983–90. https://doi.org/10.1016/j.promfg.2019.02.312.

[16] Qi Y, Xu S, Huang D. Investigation on aerodynamic performance of horizontal axis wind turbine by setting micro-plate in front of the blade leading edge. Renew Energy 2021;179:2309–21. https://doi.org/10.1016/j.renene.2021.08.035.

[17] Elsakka MM, Ingham DB, Ma L, Pourkashanian M. CFD analysis of the angle of attack for a vertical axis wind turbine blade. Energy Convers Manag 2019;182(September 2018):154–65. https://doi.org/10.1016/j.enconman.2018.12.054.

[18] Jianlong Ma, Yafan Duan, Ming Zhao, Wenchun Lv, Jianwen Wang, Qilao Meng Ke, et al. Effect of airfoil concavity on wind turbine blade performances 2019;2019. https://doi.org/10.1155/2019/6405153.

[19] Wang Y, Li G, Shen S, Huang D, Zheng Z. Investigation on aerodynamic performance of horizontal axis wind turbine by setting micro-cylinder in front of the blade leading edge. Energy 2017. https://doi.org/10.1016/j.energy.2017.10.094.

[20] Pranto RI, Inam MI. Numerical analysis of the aerodynamic characteristics of NACA-4312 airfoil 2020;1(2):29–36.

[21] Erkan O, Özkan M, Karakoç TH, Garrett SJ, Thomas PJ. Investigation of aerodynamic performance characteristics of a wind-turbine-blade profile using the finite-volume method. Renew Energy 2020;161. https://doi.org/10.1016/j.renene.2020.07.138.

[22] Liu Y, Li P, He W, Jiang K. Numerical study of the effect of surface grooves on the aerodynamic performance of a NACA 4415 airfoil for small wind turbines. J Wind Eng Ind Aerod 2020;206(May):104263. https://doi.org/10.1016/j.jweia.2020.104263.

[23] Al-jibory MW, Abed H, Shinan A, Wang L. Simulation analysis on the blade airfoil of small wind turbine simulation analysis on the blade airfoil of small wind turbine. In: IOP Conference Series: Earth and Environmental Science; 2019. https://doi.org/10.1088/1755-1315/295/2/012079.

[24] Sudhanshu SM, Sourabh RD, Sanjay NH, Shubhanga VK, Yash AK. Horizontal axis wind turbines passive flow control methods : a review horizontal axis wind turbines passive flow control methods: a review. In: IOP Conference Series Materials Science and Engineering; 2021. https://doi.org/10.1088/1757-899X/1136/1/012022.

[25] Niu W, Zhang Y, Chen H, Zhang M. Numerical study of a supercritical airfoil/wing with variable-camber technology. Chin J Aeronaut 2020;33(7):1850–66. https://doi.org/10.1016/j.cja.2020.01.008.

[26] Mourad MG, Shahin I, Ayad SS, Abdellatif OE, Mekhail TA. Effect of winglet geometry on horizontal axis wind turbine performance. Eng Reports 2020;2(1):1–19. https://doi.org/10.1002/eng2.12101.

[27] Alabi OO, Adeaga OA, Akintola SA. Numerical modeling and investigation of flow of incompressible non-Newtonian fluids through uniform slightly deformable channel. In: 2023 Int. Conf. Sci. Eng. Bus. Sustain. Dev. Goals, vol. 1, no. 1984; 2020. p. 1–6. https://doi.org/10.1109/SEB-SDG57117.2023.10124471.